Chapter 9

The Betts–Miller Scheme

ALAN K. BETTS

Atmospheric Research, Pittsford, Vermont

MARTIN J. MILLER

European Centre for Medium-Range Weather Forecasts, Reading, Berkshire, United Kingdom

9.1. Introduction

The impetus for the development of this simple lagged convective adjustment scheme came from the series of tropical field experiments in the decade 1969–79 [VIMHEX, the Venezuela International Meteorological the Hydrological Experiment in 1969 and 1972; GATE, the GARP (Global Atmospheric Research Program) Atlantic Tropical Experiment in 1974, and MONEX, the Monsoon Experiment in 1979]. Deep convection is the dominant vertical transport process in the tropics. In conjunction with the radiation field and the subsiding branches of the tropical circulations, convective processes maintain a vertical thermal structure, which is quite close to the moist adiabat through the equivalent potential temperature θ_e of the subcloud layer in the regions of deep convection. This was the basis of early cumulus parameterization schemes. Manabe (1965) proposed adjustment toward a moist-adiabatic structure to remove conditional instability in large-scale models. Kuo (1965, 1974) proposed a simple cloud model for deep convection that adjusted the atmosphere toward the saturated moist pseudoadiabat in the presence of grid-scale moist convergence. However, the mean tropical atmosphere is always cooler by several degrees in the middle troposphere than this reference moist adiabat, even in regions of vigorous convection (see Figs. 9.5–9.7). At the same time, the deep convective transports also maintain the water vapor and cloud distributions in the tropics, which in turn play a crucial role in the radiative fluxes.

One of the key objectives of GATE in 1974 was to study organized deep convection in order to test and develop convective parameterizations for numerical models (Betts 1974a). Meanwhile, the work of Ooyama (1971), Arakawa and Schubert (1974), Ogura and Cho (1973), and Yanai et al. (1973) had sparked much research to parameterize and model tropical deep convection in terms of spectral cloud ensembles with a simple entraining cloud model. Betts (1973a) had formulated deep convective transports in terms of an updraft and downdraft mass circulation using conserved variables. Diagnostic studies from GATE showed the importance of mesoscale updrafts and downdrafts in addition to convective-scale processes and the microphysical effects of freezing, melting, and water loading (Houze and Betts 1981). Similar studies from MONEX confirmed the importance of processes on many scales (Houze et al. 1981). Frank (1983) concluded from these phenomenological studies that cloud models of greater complexity might be needed to parameterize cumulus convection. Work has continued on these lines (Frank and Cohen 1987; Krueger 1988), but progress has been slow. The introduction of every new degree of freedom in a parametric cloud model requires a new closure assumption, and it remains impossible to integrate a numerical cloud model of much realism at every grid point in a global model. Typically, simplified mass flux schemes have been developed as parameterizations for operational global models—for example, Tiedtke (1989) at the European Centre for Medium-Range Forecasts (ECMWF) and Gregory and Rountree (1990) at the U.K. Meteorological Office. The reader is referred to these original papers, since this work is not summarized in this volume.

The Betts–Miller scheme was designed to represent directly the quasi-equilibrium state established by deep convection, so as to avoid the uncertainties involved in attempting to determine this state indirectly using increasingly complex cloud models, whose closure parameters can themselves ultimately be determined only by comparison with atmospheric observables. The concept of a quasi equilibrium between the convective field and the large-scale forcing was introduced for shallow convection by Betts (1973b) and for deep convection by Arakawa and Schubert (1974). The idea, in fact, has a long history (e.g., Ludlam 1966). On larger space and longer time scales, quasi equilibrium has been well established (Lord and Arakawa 1980; Lord 1982; Arakawa and Chen 1987). Quasi equilib-

rium means that the convective cloud field tightly constrains the temperature and moisture structure of the atmosphere. Arakawa and Schubert (1974) closed the problem by constraining the cloud work function. Betts and Miller (1986) chose to independently constrain the temperature and moisture structure. In the presence of extensive deep convection, the atmospheric thermal structure rather than approaching the pseudoadiabat seems to remain slightly unstable to the wet virtual adiabat at least up to the freezing level (Betts 1982, 1986; Xu and Emanuel 1989; Binder 1990). The theoretical basis for this is not completely clear. The wet virtual adiabat (Betts 1983; Betts and Bartlo 1991) includes the effect of liquid water loading, which clearly plays an important role in reducing buoyancy and updraft velocities in the weaker updrafts found in tropical cumulonimbi (Zipser and LeMone 1980). Cloud modeling studies (Cohen 1989; Cohen and Frank 1989) have shown that the quasi-equilibrium thermal state does indeed approach this wet virtual adiabat. In addition, atmospheric soundings in convective regions typically show a stable kink in the thermal structure near the freezing level, suggesting that the freezing–melting process, which is closely tied to the 0°C isotherm, also has an important control on the midtropospheric equilibrium thermal structure. Thus, it seems likely that below the freezing level both water loading and, perhaps to a lesser extent, melting of falling frozen precipitation may contribute to the observed quasi-equilibrium thermal structure, unstable to the pseudoadiabat but close to the wet virtual adiabat. Similarly, above the freezing level, the observed more stable structure is probably associated with both the freezing process and the fallout of precipitation, which reduces the liquid and ice loading on a parcel. In the Betts–Miller scheme, we chose to use the wet virtual adiabat as a reference process up to the freezing level, to link the complex physics of cloud fields to a well-defined thermodynamic reference process that appears to have an observational and some (albeit incomplete) theoretical basis. Although it can be argued with some justification that this is a semiempirical approach, our objective is a simple parameterization of complex processes on a wide range of scales. Since the observations and cloud-scale models suggest that both water loading (and therefore the microphysics) and the freezing–melting process are important in determining the thermal structure, if we do not parameterize the structure directly we must include all these processes with some realism in parametric cloud models. So far, few cumulus parameterization schemes have faced this daunting task.

Since its introduction, the scheme has been tested at ECMWF (Heckley et al. 1987) and in data assimilation studies (Puri and Miller 1990; Puri and Lonnberg 1991), and used in limited-area models (Janjic 1990), theoretical studies of hurricane development (Baik et al. 1990), and climate (Lawsen and Eliasen 1989). Here we discuss some of the improvements that have been made to the scheme since these works were published.

9.2. Observational basis

The convection scheme involves a lagged adjustment toward calculated reference profiles. The procedure selected for calculating these reference profiles was influenced by observational studies of convective equilibrium. Betts and Miller (1986) showed examples of equilibrium structure for deep and shallow convection, and subsequent papers have generally provided supporting evidence. In this section, we shall illustrate the basis of the parameterization scheme using examples from observations. The formal details of the parameterization scheme are left to sections 9.3 and 9.4.

a. Shallow scheme

Figure 9.1 shows a parametric idealization of the coupling of a temperature and dewpoint T_D structure of a convective layer to a mixing line from Betts (1985, 1986). The four points, A, B, C, and D, on the heavy dashed mixing line (a line of constant $\partial\theta/\partial q$) at a saturation pressure p^* are connected with a corresponding pair of (T, T_D) points at a pressure level p (the dashed lines) by lines of constant θ and q. Although Fig. 9.1 shows a single mixing line, the convective boundary layer (CBL) has three distinct layers, which have different characteristic values of the gradient of saturation pressure p^* with p. We define a parameter

$$\beta = \frac{\partial p^*}{\partial p}. \tag{9.1}$$

Note that the gradient with p of θ and q are linked by β to the slope of the mixing line

$$\frac{\partial \theta}{\partial p} = \beta\left(\frac{\partial \theta}{\partial p^*}\right)_M \tag{9.2a}$$

$$\frac{\partial q}{\partial p} = \beta\left(\frac{\partial q}{\partial p^*}\right)_M, \tag{9.2b}$$

where the suffix M denotes the mixing line. The parameter β represents in some sense a measure of the mixing within and the coupling between convective layers. The insert on the right of Fig. 9.1 shows β for the three layers of the schematic CBL. Here $\beta = 0$ would represent a well-mixed layer: the subcloud layer often approaches this structure. In Fig. 9.1, the subcloud layer has $0 < \beta < 1$, which represents a layer not quite mixed, in which the profiles of θ, q converge with height toward saturation on the mixing line. The lower part of the cloud layer is drawn with $\beta = 1$; this is a partially mixed structure in which the θ, q (or T, T_D) profiles are approximately parallel to the mixing line. Near cloud top $\beta > 1$; this represents the divergence

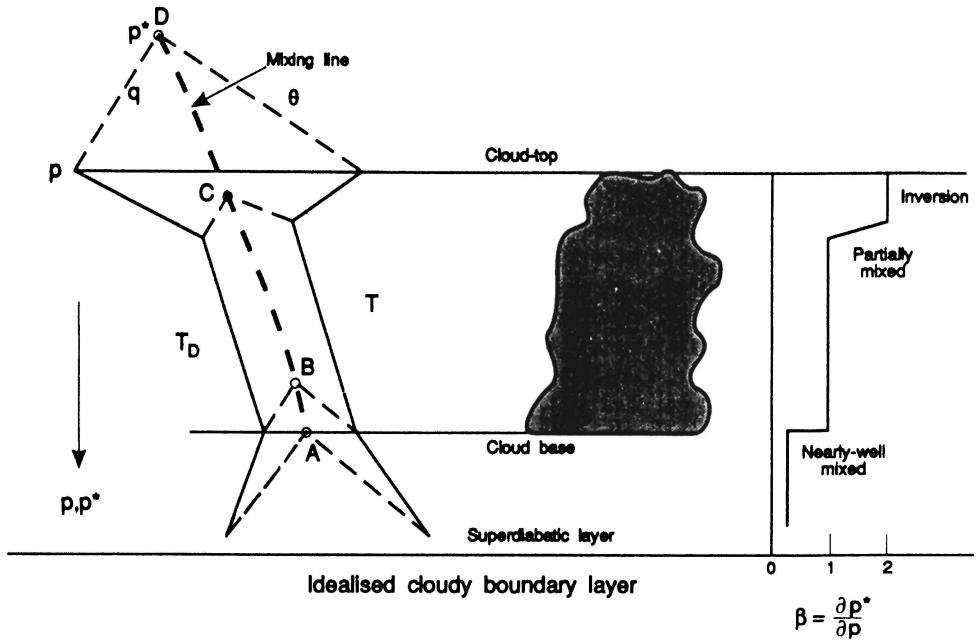

FIG. 9.1. Relationship between mixing line, temperature, and dewpoint, and a mixing parameter β for an idealized convective boundary layer. The light dashed lines are lines of constant potential temperature θ and mixing ratio q (from Betts 1986).

of θ and q from the mixing line that is characteristic of the transition through an inversion at the top of a convectively mixed layer to the free atmosphere. Figure 9.2 shows an actual mean CBL sounding for the equatorial Pacific from Betts and Albrecht (1987) as profiles of saturation equivalent potential temperature θ_{es} and equivalent potential temperature θ_e with pressure.

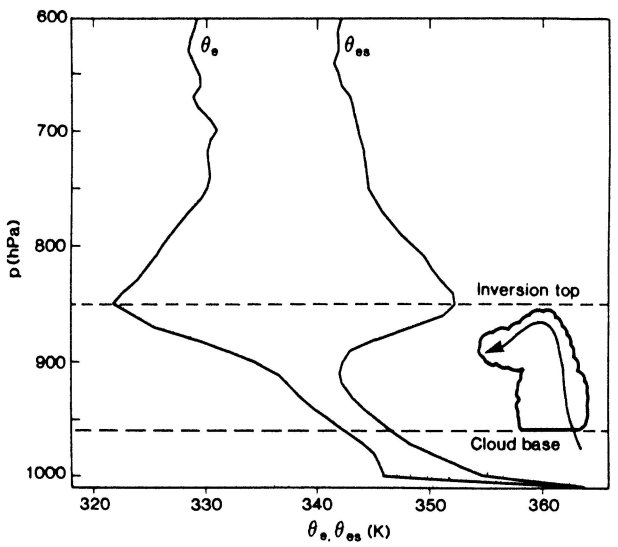

FIG. 9.2. Mean profiles of equivalent potential temperature θ_e and saturation equivalent potential temperature θ_{es} through an oceanic convective boundary layer (data from Betts and Albrecht 1987).

Cloud base is near 960 hPa, and the main trade-wind inversion is between 890 and 850 hPa in this average: the minimum in θ_{es} is a little lower at 910 hPa. The top of the inversion is marked by a maximum in θ_{es} and a minimum in θ_e, which means that the air just above the CBL has a minimum in relative humidity. This is a typical structure in the trade winds of the central equatorial Pacific. Figure 9.3 shows the same mean sounding on a conserved variable diagram: a θ^*–q^* plot, which for this unsaturated sounding is identical to a θ–q plot. The open circles are (θ, q) plotted every

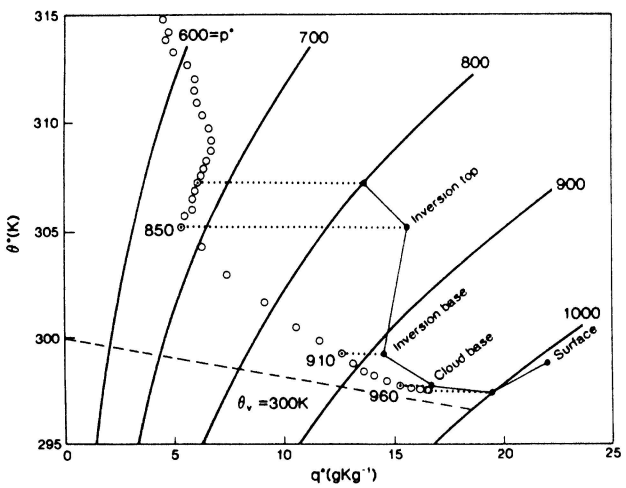

FIG. 9.3. Conserved variable plot (θ^*, q^*) of data from Fig. 9.2.

10 hPa from 1000 hPa. Selected levels are marked for cloud base, (960 hPa), θ_{es} minimum (910 hPa), and inversion top (850 hPa). There is a sharp kink at inversion top that marks the top of the convectively mixed layer. Within the CBL the profile has two parts. Below cloud base the θ–q structure is parallel to a line of neutral density for dry convection, the dry virtual adiabat (Betts and Bartlo 1991); a line of θ_v = 300 K is shown (dashed). Between cloud base and inversion top the profile can be approximated by a linear mixing line, signifying a layer in which convection is mixing air sinking through the trade inversion with air in the subcloud layer, itself coupled to the ocean. In this cloud layer the profile is actually slightly curved, because the time scale of the convective mixing is of order many hours, during which time radiative cooling reduces θ at constant q (Betts 1982).

The open circles in Fig. 9.3 are data plotted at their saturation level p^*, θ^*, and q^*. The profile of $\theta(p)$ is also shown on this figure by solid circles at selected levels, joined by light lines. Each $\theta(p)$ point shown is connected by a dotted line at constant θ to the corresponding saturation point at p^* (the corresponding lifting condensation level). The solid circle marked surface represents saturation at the ocean surface temperature and pressure (1010 hPa). Note that the trade inversion, which is very marked on a $\theta(p)$ or $\theta_{es}(p)$ plot (Fig. 9.2), appears only on a θ^*–q^* plot as a wider spacing of points on the same mixing line. The air above the CBL has its own characteristic structure, which here has almost constant p^*. Betts and Albrecht (1987) suggested that this air had sunk over many days, originating from deep convective outflows near the freezing level.

Figure 9.4 shows the actual plot of $\beta = \partial p^*/\partial p$ for this observed profile. The inversion layer has a large value of β peaking near 9.5, while the cloud layer has nearly constant β near 1.15. The subcloud layer has smaller values of β, but the subcloud values are probably a little large, because of averaging of the poor vertical resolution dropsonde data (Betts and Albrecht 1987).

The shallow convection scheme in the present ECMWF code does not treat convection in the subcloud layer; this is done by a separate diffusion scheme. We then specify β = 1.2 from cloud base to cloud top, as a reasonable approximation to the observational studies in Betts and Albrecht (1987). Cloud top is defined as the level below buoyancy equilibrium (see section 9.3c). This means that the subsaturation parameter $\mathcal{P} = p^* - p$ increases slowly (in magnitude) in the cloud layer since $\partial\mathcal{P}/\partial p = \beta - 1 = 0.2$. The value of $\mathcal{P}$ is not specified but implicitly determined by the two separate integral energy constraints on water vapor and enthalpy (see section 9.3f), since we assume shallow convection does not precipitate. A linear approximation to the slope $\partial\theta/\partial p$ of the mixing line is computed between low-level air and air from two levels

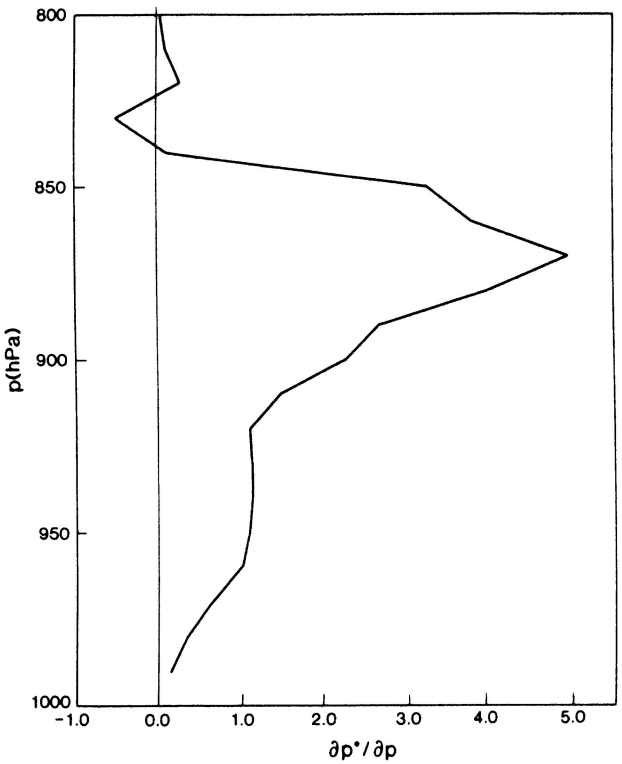

FIG. 9.4. Profile of parameter $\beta = \partial p^*/\partial p$ (the gradient of saturation pressure with pressure) through the convective bondary layer shown in Fig. 9.2.

above cloud top. One can see in Fig. 9.3 that a low vertical resolution model using data perhaps 30–50 hPa above the inversion top will tend to overestimate the mixing-line slope. Therefore, we have introduced a weighting parameter (presently 0.85) to reduce the mixing-line slope to compensate for this (see section 9.3f). At the model level just above cloud top, an intermediate value of β is estimated to smooth the transition at cloud top. A generalization of the parametric model may well be useful in which β is a function of mixing-line slope (Betts 1985), but this has not been implemented.

b. Deep scheme

The deep scheme adjusts toward reference profiles characteristic of deep convective equilibrium. Figure 9.5 shows average profiles of the temperature difference ΔT_w from the moist pseudoadiabat through cloud base for the hurricane eyewall composite (solid) and 2° radius composite (dashed) from Frank (1977). The mean sounding for this extreme convective situation is cooler than the pseudoadiabat throughout the troposphere, reaching a maximum in ΔT_w, corresponding to a minimum in θ_{es}, at 500 hPa, a little above the freezing level. The wet virtual adiabat is shown dotted. This is the neutral density curve for the reversible adiabat in

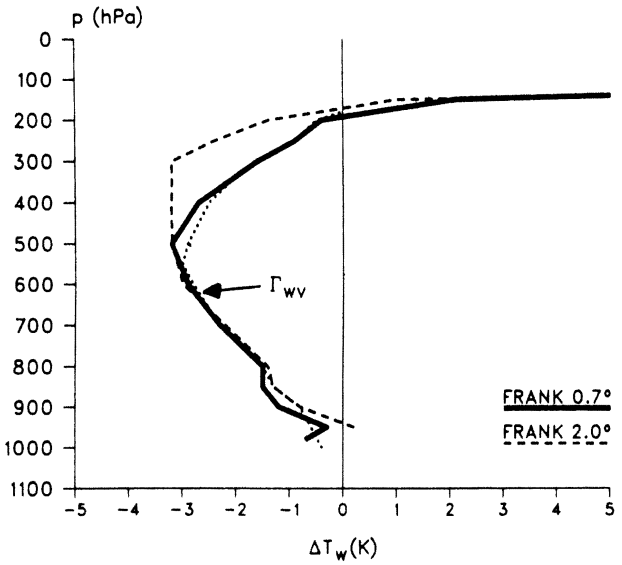

FIG. 9.5. Profile of ΔT_w (temperature difference between sounding and moist pseudoadiabat through cloud base) against pressure for two hurricane averages (data from Frank 1977).

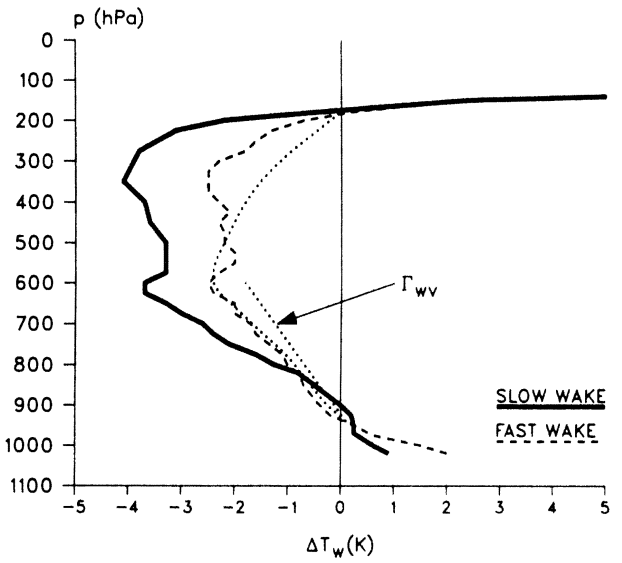

FIG. 9.6. As Fig. 9.5 for two GATE averages (data from Barnes and Sieckman 1984).

which the liquid water loading is included. The temperature profile up to the freezing level is quite close to this reference adiabat. The dotted profile above the freezing level is a quadratic fit between the freezing level and the outflow equilibrium level. The dashed profile, at 2° radius from the storm center, is a little more unstable below the freezing level, and it is cooler above than the eyewall composite. Figure 9.6 shows a second pair of curves for the wake of slow-moving (solid) and fast-moving (dashed) GATE lines from Barnes and Sieckman (1984). They are similar to the hurricane composites. The slow-moving composite has a slope above cloud base (near 950 hPa) roughly 1.3 times that of the wet virtual adiabat (dotted), while the fast-moving composite has a more unstable structure with a slope twice that of the wet virtual adiabat in the lower troposphere. Figure 9.7 shows a composite of 24 soundings within and in the vicinity of eight large storm systems (area greater than 2000 km^2) in Venezuela (see Betts 1976). Again the profiles are similar to Figs. 9.5 and 9.6, although the cloud base over land is higher, near 850 mb. The slope of ΔT_w up to the freezing level is 2.2 times that of the wet virtual adiabat. The data in Binder (1990) over Switzerland are similar. The profile above the freezing level is not far from the quadratic curve shown dotted.

Figure 9.8 shows the mean profiles of $\mathcal{P}$ for the five averages shown. Unlike Figs. 9.5–9.7 for the thermal structure, which have some qualitative similarities, there is a large variation in moisture between the averages for different types of storms and regimes. The fast-moving storms tend to have stronger low-level downdrafts, which dry out the lower troposphere, but inject more moisture into the upper troposphere, while slow-moving systems over the ocean (and over land, not shown) tend to have moister outflows in the lower troposphere. In the present version of the scheme, we use a simple mean profile (heavy line), which has a minimum at the freezing level and a linear variation above and below.

9.3. Original Betts–Miller scheme

The scheme was designed to adjust the atmospheric temperature and moisture structure back toward a ref-

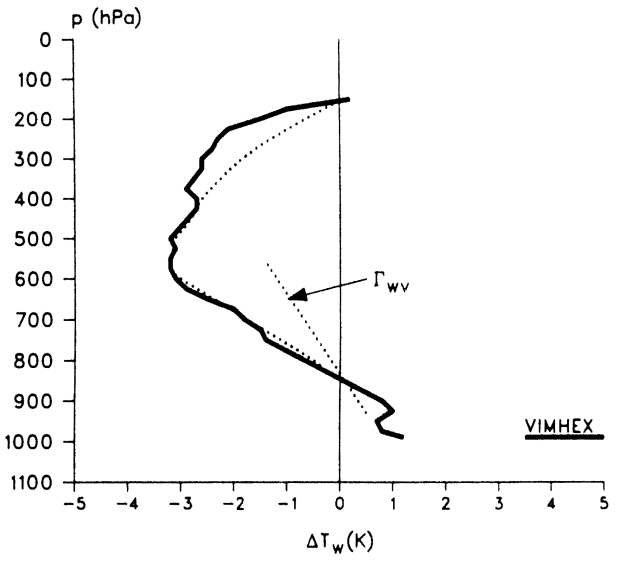

FIG. 9.7. As Fig. 9.6 for average of 24 soundings in the outflow of eight large storms over Venezuela (data from Betts 1976).

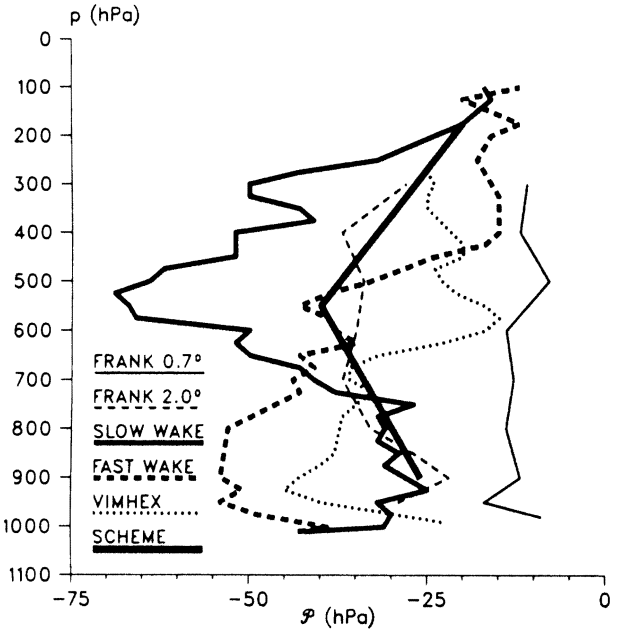

FIG. 9.8. Profile of saturation pressure departure ($\mathcal{P} = p^* - p$) with pressure for the five convective averages, and the profile used by the scheme.

erence quasi-equilibrium thermodynamic structure in the presence of large-scale radiative and advective processes. Two distinct reference thermodynamic structures (which are partly specified and partly internally determined) are used for shallow and deep convection. We have subsequently introduced a revised low-level adjustment to simulate a downdraft mass flux into the boundary layer (BL): this is discussed in section 9.4. Formally the convection scheme involves four parts: the specification of τ the adjustment time scale, finding cloud base and cloud top, determining the reference profiles for deep and shallow convection, and the method of distinguishing between deep and shallow convection. Figure 9.9 shows a flow diagram for the overall scheme. We shall discuss the formal structure of a lagged adjustment scheme first and then outline the components.

a. Formal structure

If we denote a saturation point (θ^*, q^*) by a two-dimensional vector $\mathbf{S}$ (Betts 1983), the large-scale thermodynamic tendency equation can be written as

$$\frac{\partial \bar{\mathbf{S}}}{\partial t} = -\mathbf{V}\cdot\nabla\mathbf{S} - \bar{\omega}\frac{\partial \bar{\mathbf{S}}}{\partial p} - g\frac{\partial \mathbf{N}}{\partial p} - g\frac{\partial \mathbf{F}}{\partial p}, \quad (9.3)$$

where $\mathbf{N}$, $\mathbf{F}$ are the net radiative and convective fluxes (including the precipitation flux). The convective flux divergence is parameterized as

$$-g\frac{\partial \mathbf{F}}{\partial p} = \frac{\mathbf{R} - \bar{\mathbf{S}}}{\tau}, \quad (9.4)$$

where $\mathbf{R}$ is the reference quasi-equilibrium thermodynamic structure and τ is a relaxation or adjustment time representative of the convective and unresolved mesoscale processes.

Simplifying the large-scale forcing to the vertical advection and combining (9.3) and (9.4) gives

$$\frac{\partial \bar{\mathbf{S}}}{\partial t} = -\bar{\omega}\frac{\partial \bar{\mathbf{S}}}{\partial p} + \frac{\mathbf{R} - \bar{\mathbf{S}}}{\tau}. \quad (9.5)$$

If the large-scale forcing is steady on time scales longer than τ, then the atmosphere will reach a quasi equilibrium with $\partial\bar{\mathbf{S}}/\partial t \approx 0$. Then

$$\mathbf{R} - \bar{\mathbf{S}} \approx \bar{\omega}\left(\frac{\partial \bar{\mathbf{S}}}{\partial p}\right)\tau. \quad (9.6)$$

In a T-106 global model we use τ = 1 h (see below). This means that $\mathbf{R} - \bar{\mathbf{S}}$ corresponds to one hour's forcing by the large-scale fields, including radiation. For deep convection the atmosphere will therefore remain slightly cooler and moister than $\mathbf{R}$. Furthermore, for small τ, the atmosphere will approach $\mathbf{R}$, so that we may substitute $\mathbf{S} \approx \mathbf{R}$ in the vertical advection term, giving

$$\mathbf{R} - \bar{\mathbf{S}} \approx \omega\tau\frac{\partial \mathbf{R}}{\partial p}, \quad (9.7)$$

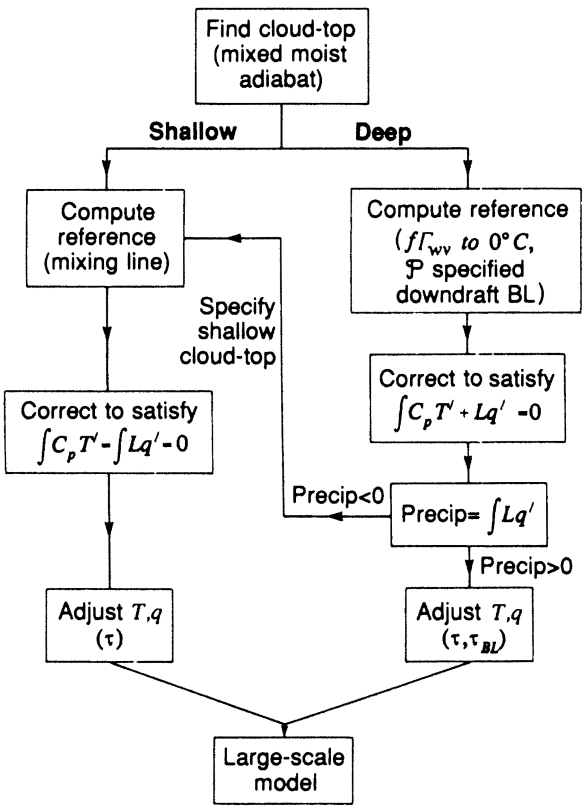

FIG. 9.9. Flowchart for Betts–Miller convection scheme.

from which the convective fluxes can be approximately expressed using (9.2) as

$$\mathbf{F} = \int \frac{\mathbf{R} - \bar{\mathbf{S}}}{\tau} \frac{dp}{g} \approx \int \bar{\omega} \frac{\partial \mathbf{R}}{\partial p} \frac{dp}{g}. \quad (9.8)$$

Equation (9.8) shows that the structure of the convective fluxes is closely linked to the structure of the specified reference profile **R**. By adjusting toward an observationally realistic thermodynamic structure **R**, we simultaneously constrain the convective fluxes including precipitation to have a structure similar to those derived diagnostically from (9.3), or its simplified form (9.8), by the budget method (Yanai et al. 1973).

Substituting p and p^* in (9.7) gives (suffix R for the reference profile)

$$\mathcal{P}_R - \bar{\mathcal{P}} = p_R^* - \bar{p}^* \approx \omega\tau \frac{dp_R^*}{dp} \approx \omega\tau, \quad (9.9)$$

since $1 < dp_R^*/dp < 1.1$ for the deep reference profiles that are used. Rearranging gives an approximate value for

$$\bar{\mathcal{P}} \approx \mathcal{P}_R - \omega\tau. \quad (9.10)$$

This means that while the deep convection scheme is operating the mean vertical advection (if steady for time periods longer than τ) will shift the grid-scale value of $\bar{\mathcal{P}}$ away from the specified reference state $\mathcal{P}_R$ toward saturation by approximately $\omega\tau$ mb. Thus, although we specify in the present simple scheme a constant global value of the reference structure $\mathcal{P}_R$, $\bar{\mathcal{P}}$ does have a spatial and temporal variability in the presence of deep convection related to that of $\bar{\omega}$.

b. *Choice of* τ

The role of convective parameterization in a global model is to produce precipitation before grid-scale saturation is reached, both to simulate the real behavior of atmospheric convection and also to prevent grid-scale instability associated with a saturated conditionally unstable atmosphere. We can see from (9.10) that if the convection scheme is to prevent grid-scale saturation ($\bar{\mathcal{P}} = 0$), there is a constraint on τ—$\tau < \mathcal{P}_R/\omega_{max}$, where ω_{max} is a typical maximum ω in, say, a major tropical disturbance. With $\mathcal{P}_R \sim -40$ mb in the middle troposphere, we have found that this suggests an upper limit on τ, which is approximately 2 h for the ECMWF T-63 spectral model and 1 h for the T-106 model, with smaller values at higher resolutions. We recommend that τ should be set so that the model atmosphere nearly saturates on the grid scale in major convective disturbances. This is an empirical approach to the adjustment time scale by convection. In a numerical model a lagged adjustment, rather than a sudden adjustment at a single time step, has the advantage of smoothness, with less of a tendency to "blink" on and off at grid points in a physically unrealistic way. We have subsequently introduced a distinct boundary layer, τ_{BL}, connected physically to downdraft mass flux and evaporation. Typically $\tau_{BL} > \tau$ (see section 9.4). However, we have as yet no satisfactory physical model for τ, since in current global or regional models the convection scheme is parameterizing processes on both the cloud scale and the unresolved mesoscale, processes that themselves have a range of time scales. We use τ = 2 h for shallow convection.

c. *Cloud base and cloud top*

Cloud base is found by lifting air from the lowest model level to saturation and then testing for buoyancy at the next model level. We look for the lowest cloud base. Air is lifted from higher model levels if air from the lowest level is not buoyant. Convection from middle-tropospheric levels is also permitted if air lifted from the boundary layer is not buoyant. The moist adiabat corresponding to buoyant ascent is computed. The temperature of a partially mixed parcel (see section 9.3d) is then compared with the sounding at each level until a level of negative buoyancy is found. One level below is the initial choice of cloud top, p_T.

d. *Cloud-top mixing algorithm*

Subsequent to Betts and Miller (1986), we have introduced an algorithm to find cloud top that combines the moist adiabat with cloud-top mixing in an effort to pick up weak trapping inversions, which are not well resolved in the vertical.

Figure 9.10 shows the construction following Fig. 5 of Betts (1982). We linearize the mixing line (heavy dashed line) between the saturation point of cloud-base air at presure p_B and the environment at a pressure level p_K. We then find a cooler cloud parcel ascent

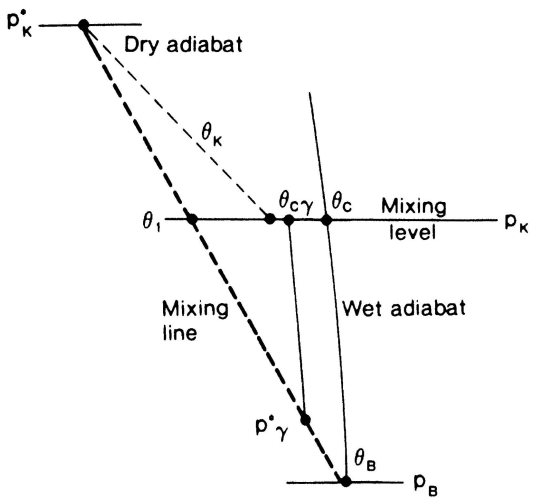

FIG. 9.10. Schematic showing thermodynamics of cloud-top mixing algorithm.

temperature $\theta_{c\gamma}$ at level K by mixing a fraction γ of the environmental air at that level with air that has risen adiabatically from cloud base (θ_c). This mixture has a saturation point at p^*_γ on the mixing line

$$p^*_\gamma = p_B - \gamma \Delta p^*, \tag{9.11}$$

where Δp^* is the difference in saturation level $p_B - p^*_K$ between cloud base and air at p_K. The potential temperature $\theta_{c\gamma}$ of this cloudy mixture at p_k can be written

$$\theta_{c\gamma} = \theta_c + (\theta_1 - \theta_c)\left(\frac{\gamma}{\gamma_c}\right), \tag{9.12}$$

where $\gamma_c = \Delta p / \Delta p^*$, $\Delta p = p_B - p_K$, and θ_1 is the cool potential temperature of the mixture that is just saturated at p_K. For the mixture to be cloudy, we require $\gamma < \gamma_c$. Finally θ_1, which lies on the same mixing line, is given by

$$\theta_1 = \theta_B + (\theta_K - \theta_B)\gamma_c. \tag{9.13}$$

Combining (9.11) and (9.12) gives the temperature of the mixture

$$\theta_{c\gamma} = \theta_c\left(1 - \frac{\gamma}{\gamma_c}\right) + \gamma\theta_K + \theta_B\left(\frac{\gamma}{\gamma_c} - \gamma\right). \tag{9.14}$$

We perform this mixing calculation *separately* at each level, and look for a level of negative buoyancy, by comparing the mixed cloud temperature with the sounding temperature: that is, we look for a level where $\theta_{c\gamma} - \theta_K < 0$. We have used a value of $\gamma = 0.2$.

e. *Selection of deep or shallow convection*

Shallow nonprecipitating convection is first separated from deep precipitating convection by using a cloud-top threshold: $p_{\mathrm{SHAL}} \sim 700$ mb (strictly the hybrid coordinate of approximately 0.7). If $p_T > p_{\mathrm{SHAL}}$, then it is a shallow convection point. If $p_T < p_{\mathrm{SHAL}}$, then we call this initially a deep convection point. At this stage the separation of deep and shallow convection is based purely on a static thermodynamic criterion (equilibrium cloud top: see Fig. 9.9), not on any dynamic constraint (such as moisture convergence as in Kuo's scheme). We proceed to set up deep or shallow reference profiles and compute the convective adjustments and precipitation. A dynamic constraint enters at this point, because often the convective adjustment for a deep convective point gives "negative precipitation," which is clearly physically unrealistic. These points arise because in regions of weak subsistence the model may not resolve the low-level inversions that in the tropics cap the convective boundary layer, so that the scheme first attempts a deep convective adjustment. We then swap these points from the deep to the nonprecipitating shallow scheme as indicated in Fig. 9.9, with a specified shallow cloud top, and compute new reference profiles.

f. *Reference thermodynamic profiles for shallow convection*

Shallow convection is parameterized in terms of an approach toward a mixing-line structure. The scheme computes the slope of the mixing line from cloud base to two levels above cloud top (p_{T+2}). An exact method would use saturation level θ^*, q^* to compute $(\partial\theta^*/\partial q^*)_M$, but for computational simplicity, we compute a linearized slope with respect to pressure $(\partial\theta^*/\partial p^*)_M = (\theta_{T+2} - \theta_B)/(p^*_B - p^*_{T+2})$. Because of the relatively poor vertical resolution in the global model above the CBL, we multiply $(\partial\theta^*/\partial p^*)_M$ by a coefficient (currently 0.85) to reduce the tendency to overestimate $(\partial\theta^*/\partial p^*)_M$ using model level data (see Fig. 9.3, for example). We define

$$M_\theta = 0.85\left(\frac{\partial\theta^*}{\partial p^*}\right)_M, \tag{9.15}$$

and then we construct first-guess profiles (superscript 1) of θ_R, q_R from

$$\theta^1_R(p) = \bar{\theta}(p_B) + \beta M_\theta(p - p_B), \tag{9.16}$$

where $\beta = \partial p^*/\partial p$ is specified. The current value is $\beta = 1.2$. In the current (experimental) ECMWF code, we continue the reference profiles to one higher level p_{T+1} using a value of β calculated for the inversion, in order to smooth the transition through the cloud-top inversion. The first-guess moisture reference profile is then computed from T_R and $p^*_R = p^*_B + \beta(p - p_B)$. These first-guess profiles are then corrected to satisfy the two separate energy constraints

$$\int_{p_B}^{p_{T+1}} c_p(T_R - \bar{T})dp = \int_{p_B}^{p_{T+1}} L(q_R - \bar{q})dp = 0, \tag{9.17}$$

so that the condensation (and precipitation) rates are zero when integrated from cloud base p_B to one level above cloud top p_{T+1}. This implies that the shallow convection scheme does not precipitate but simply redistributes heat and moisture in the vertical. This is done by correcting the first-guess values of T_R, q_R at each level by

$$\Delta T = \frac{1}{p_B - p_{T+1}} \int_{p_{T+1}}^{p_B} (T - T^1_R)dp \tag{9.18a}$$

$$\Delta q = \frac{1}{p_B - p_{T+1}} \int_{p_{T+1}}^{p_B} (q - q^1_R)dp. \tag{9.18b}$$

By making this correction independent of pressure, we preserve (to sufficient accuracy) the slope of the reference profiles, and a value of $\mathcal{P}$ independent of pressure. Since we have two constraints, it is not necessary to constrain $\mathcal{P}$ (unlike for deep convection where only one energy constraint is available; see next section). Instead, after we apply the corrections ΔT, Δq, the

adjustment closely conserves the vertically averaged value of $\mathcal{P}$ through the shallow convective layer.

g. Reference profiles for deep convection

We first construct a first-guess thermal profile, followed by a first-guess moisture profile, and then these are corrected to satisfy moist static energy balance.

The reference profile for θ is computed up to the freezing level as a fraction of the slope of the moist pseudoadiabat. Defining $\Gamma_m = \partial\theta/\partial p$ for the moist adiabat, we set the first-guess profile at

$$\theta_R^1(p) = \bar{\theta}_B + 0.85\Gamma_m(p_B - p) \qquad (9.19)$$

for $p_B < p < p_F$.

A coefficient of 0.9 corresponds to the slope of the wet virtual adiabat: the coefficient of 0.85 is a more unstable profile equivalent to ΔT_w having a slope 1.5 times that of the wet virtual adiabat in Figs. 9.6 and 9.7. In the original scheme we extended this profile down to one level above the surface and chose a value of $\bar{\theta}_B$ near cloud base. In the current revised scheme (see section 9.4), the deep reference profile near the surface is computed differently from an unsaturated downdraft profile, and $\bar{\theta}_B$ is at a level just above this new boundary layer.

Above the freezing level, the profile returns to the moist pseudoadiabat at cloud top. The interpolation is done quadratically in terms of the temperature difference from the wet adiabat, so that

$$T_R^1(p) = T_c(p) + [T_R(p_F) - T_c(p_F)](1 - y^2), \qquad (9.20)$$

where $y = (p_F - p)/(p_F - p_T)$. This involves several small changes from Betts and Miller (1986), in which the reference profile returned linearly to the environmental temperature at cloud top, and θ rather than T was used for the interpolation.

The moisture profile q_R is then computed from the temperature profile by specifying $\mathcal{P} = (p^* - p)$ at three levels—cloud base $\mathcal{P}_B$, the freezing level $\mathcal{P}_F$, and cloud top $\mathcal{P}_T$—with linear gradients between.

For $p_B > p > p_F$, this gives

$$\mathcal{P}_R(p) = \frac{(p_B - p)\mathcal{P}_F + (p - p_F)\mathcal{P}_B}{p_B - p_F}, \qquad (9.21a)$$

and for $p_F > p > p_T$,

$$\mathcal{P}_R(p) = \frac{(p_F - p)\mathcal{P}_T + (p - p_T)\mathcal{P}_F}{p_F - p_T}. \qquad (9.21b)$$

In the present version of the model, the values chosen are $(\mathcal{P}_B, \mathcal{P}_M, \mathcal{P}_T) = (-25\text{ mb}, -40\text{ mb}, -20\text{ mb})$. The first-guess profiles of (T_R^1, q_R^1) are then modified until they satisfy the total enthalpy constraint

$$\int_{p_0}^{p_T} (k_R - \bar{k})dp = 0, \qquad (9.22)$$

where $k = c_pT + Lq$ and the integral is through the depth of the convective layer.

The procedure is to calculate

$$\Delta k = \frac{1}{\Delta p_c}\int_{p_0}^{p_T} (k_R - \bar{k})dp, \qquad (9.23)$$

where Δp_c is the depth of the deep convective layer included in the integral; T_R is then corrected at each level, at constant $\mathcal{P}$, so as to change k_R by Δk, independent of pressure. This energy correction is iterated once. In Betts and Miller (1986), this correction was applied at all levels except cloud top and a shallow surface layer. In the present scheme the correction is applied at all levels above a model boundary layer, where the adjustment is linked to the downdraft thermodynamics. This involves a modification to (9.23) to include the two adjustment time scales [Eq. (9.30) in section 9.4].

h. Convective tendencies and precipitation

The convective adjustment, $(\mathbf{R} - \mathbf{S})/\tau$, is then applied to the separate temperature and moisture fields as two tendencies (suffix cu for cumulus convection):

$$\left(\frac{\partial T}{\partial t}\right)_{cu} = \frac{T_R - \bar{T}}{\tau}, \qquad (9.24a)$$

$$\left(\frac{\partial q}{\partial t}\right)_{cu} = \frac{q_R - \bar{q}}{\tau}. \qquad (9.24b)$$

The precipitation rate is given by

$$\text{PR} = \int_{p_0}^{p_T}\left(\frac{q_R - \bar{q}}{\tau}\right)\frac{dp}{g} = -\frac{c_p}{L}\int_{p_0}^{p_T}\left(\frac{T_R - \bar{T}}{\tau}\right)\frac{dp}{g}. \qquad (9.25)$$

No liquid water is stored in the present scheme, and the deep convective adjustment is suppressed if it ever gives PR < 0. These terms are slightly modified in the present scheme, which has a distinct adjustment in the BL (see section 9.4). If PR < 0, the shallow cloud scheme is called. Since a shallow convective cloud top has not previously been found from a buoyancy criterion, at present we specified a shallow cloud top. We intend to determine the depth of the CBL from a second thermodynamic criterion, by setting shallow cloud top at the base of the layer that has a maximum of $\partial p_K^*/\partial p_K$. This identifies the top of any moist layer that is capped by a sharp increase of θ or decrease of q. This has not yet been implemented.

Note that this scheme handles the partition between moistening of the atmosphere and precipitation in a quite different way from, say, Kuo's scheme, which specifies a partitioning of the moisture convergence. Given moisture convergence and, say, mean grid-scale upward motion, the model atmosphere moistens with no precipitation until a threshold is reached, qualita-

tively related to a mean value of $\mathcal{P}_R$, when precipitation starts. However, the model atmosphere continues to moisten (given steady-state forcing) until (9.10) is satisfied, when the moistening ceases, and the "converged moisture" is then all precipitated. If the forcing ceases ($\omega \to 0$), then precipitation continues for a while, until the atmosphere has dried out to the reference profile again. We are essentially controlling (through $\mathcal{P}_R$) the relative humidity of air leaving convective disturbances. In medium range, and particularly climate integrations of a global model, this seems a better way of maintaining the long-term moisture structure of the atmosphere than through constraints on the partition of moisture convergence. The water vapor distribution in tropics is crucial to the long-term radiative balance and at present we have insufficient data, particularly in the upper troposphere, to develop improved models. Clearly the parameterization of the moisture transport or the equilibrium moisture structure is a difficult problem. It depends on the moisture transport from primarily the subcloud layer, and the efficiency of the precipitation process, which in turn depends on the cloud and mesoscale dynamics and microphysics. We know qualitatively that more energetic convective systems typically in sheared flows and over land tend to have lower precipitation efficiencies (Fritsch and Chappell 1980), both because more condensed water is evaporated in downdrafts and because more ice is ejected at anvil levels. Figure 9.8 gives some indication of this complexity. However, the Betts–Miller scheme at present simplifies this complexity for deep convection by specifying a single reference moisture structure in terms of the saturation pressure deficit $\mathcal{P}_R$.

9.4. Modification to include downdraft mass flux boundary layer

One of the weaknesses of the original Betts–Miller (1986) scheme was that the adjustment near the surface was not well constrained. The reference profile was defined to produce a stabilization near the surface to mimic downdrafts. In practice, in the original scheme, the first-guess reference profile was started with the mean temperature at the next to lowest level, so that the adjustment at this level then depended solely on the energy correction. This was typically negative, but it was not well constrained by any physical model. In fact the deep convective interaction with the BL is crucial, especially over the oceans, where the surface temperature is constrained. As a result the scheme was modified to explicitly introduce the low-level cooling and drying by a downdraft mass flux. Observational studies have long shown the crucial role of these downdrafts in the subcloud layer interaction (e.g., Zipser 1969, 1976; Betts 1973a, 1976). To keep the parameterization simple, we define a simple unsaturated downdraft thermodynamic path and inject downdraft air with constant divergence into the three lowest model levels. Thus, for the three lowest model levels we introduce a different reference profile, related to a simple unsaturated downdraft. We also introduce a different adjustment time scale for this BL, related to the divergence of the downdraft mass flux, which is taken independent of height in the BL. The BL time scale (related to downdraft mass flux) is determined by one new closure that couples the evaporation in the downdraft to the precipitation: this represents a measure for precipitation efficiency.

a. Downdraft thermodynamics

Evaporation into downdrafts depends on complex dynamical and microphysical processes (e.g., Kamburova and Ludlam 1966; Betts and Silva Dias 1979). These we shall simplify to an unsaturated downdraft reference profile, which starts at a downdraft inflow level with the mean properties at that level and descends at constant θ_e and constant subsaturation: that is, the temperature and moisture paths are parallel to a moist adiabat. In the present code, the downdraft originates at a single level near 850 mb. Figure 9.11 shows the thermodynamics schematically. The reference profile, T_R, q_R, for the three lowest model levels (K to $K-2$ in Fig. 9.11) are set equal to the downdraft outflow properties:

$$T_R = T_{DN} = \bar{T}_{IN} + \Delta T_c, \tag{9.26a}$$

$$q_R = q_{DN} = \bar{q}_{IN} + \Delta q_c, \tag{9.26b}$$

where $\bar{T}_{IN}$, $\bar{q}_{IN}$ are the grid-mean values at the downdraft inflow level and ΔT_c, Δq_c are the changes of T, q along the downdraft descent path (defined positive). For computational efficiency we used the profiles of T_c, q_c on the ascent moist adiabat through cloud base, which are available at all levels. The approximation of

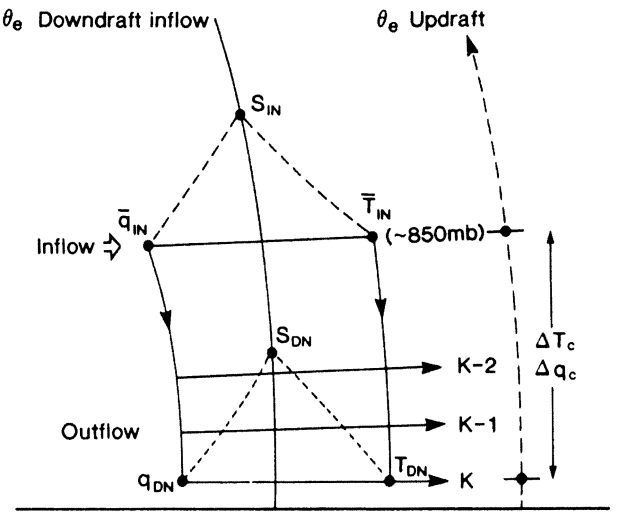

FIG. 9.11. Schematic showing thermodynamics of unsaturated downdraft model.

using a different (warmer) moist adiabat is small compared with the uncertainties in the precipitation efficiency (see below). This simple downdraft parameterization has other advantages besides being computationally efficient. It couples the relative humidity in the BL to the constrained subsaturation $\mathcal{P}$ at higher levels and gives tendencies toward a subsaturated moist-adiabatic structure [see Eq. (9.28)]. In the BL, the tendencies due to cumulus convection are

$$\left(\frac{\partial T}{\partial t}\right)_{cu} = \frac{T_R - \bar{T}}{\tau_{BL}} = \frac{\Delta T_c - \Delta \bar{T}}{\tau_{BL}} \quad (9.27a)$$

$$\left(\frac{\partial q}{\partial t}\right)_{cu} = \frac{q_R - \bar{q}}{\tau_{BL}} = \frac{\Delta q_c - \Delta \bar{q}}{\tau_{BL}}, \quad (9.27b)$$

where τ_{BL} is the adjustment time of BL, discussed in the next section, and $\Delta\bar{T}$, $\Delta\bar{q}$ are the vertical differences in the mean structure between downdraft inflow and BL outflow levels. The BL tendencies become zero if

$$\Delta\bar{T} = \Delta T_c,$$

$$\Delta\bar{q} = \Delta q_c, \quad (9.28)$$

that is, if the mean profiles become parallel to the moist adiabat. (The downdraft will not be saturated, however, unless the downdraft inflow is saturated.) Typically, unless (9.28) is achieved, $\Delta\bar{T} > \Delta T_c$ and $\Delta\bar{q} > \Delta q_c$, and the downdraft cools and dries the BL.

b. Boundary-layer adjustment time τ_{BL}

This is computed by coupling the evaporation into the downdraft to the precipitation rate (PR). We define

$$\text{EVAP} = \int_{p_0}^{p_{BL}} (\nabla \cdot \mathbf{V})_D \Delta q_c \frac{dp}{g} = \alpha \text{PR}, \quad (9.29)$$

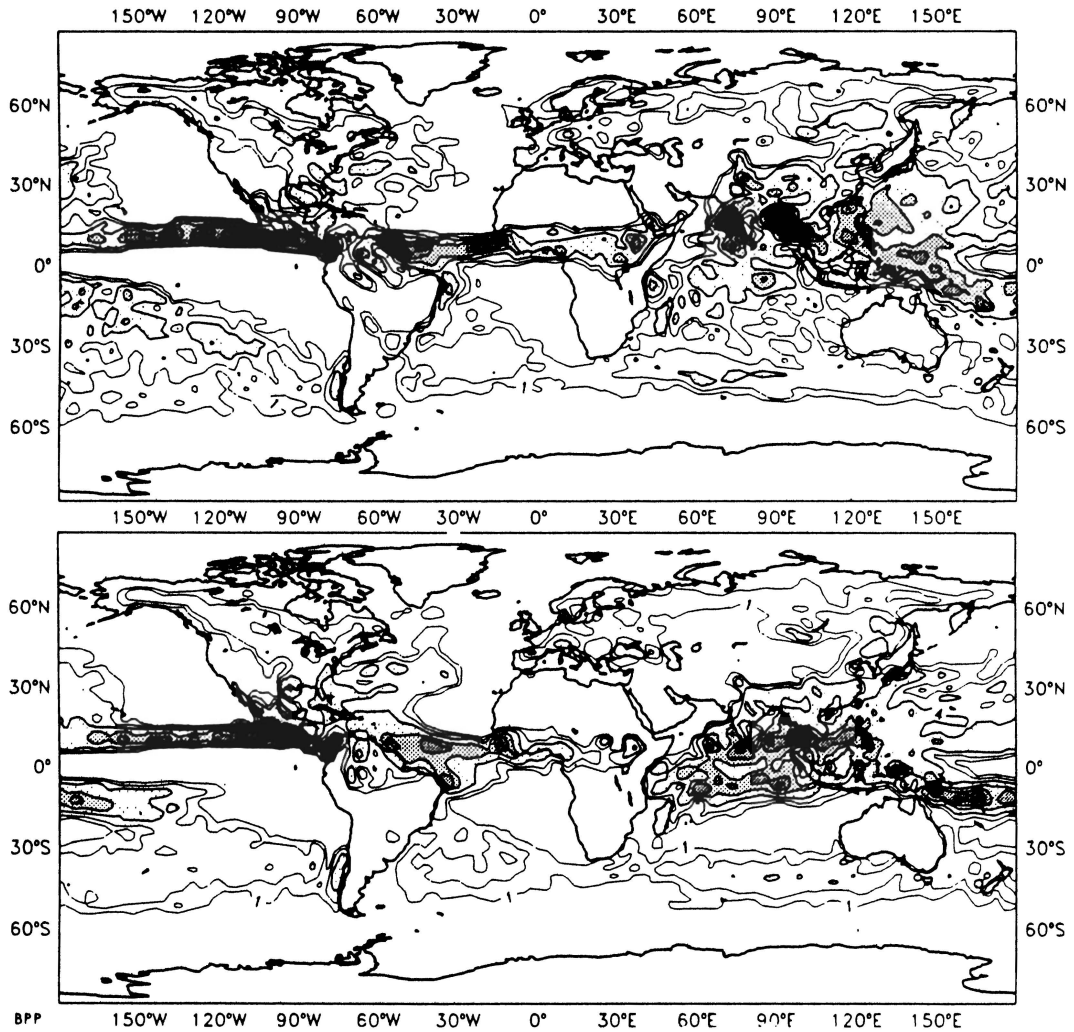

FIG. 9.12. Global map of 90-day convective precipitation for adjustment scheme (upper panel) and operational model (lower panel).

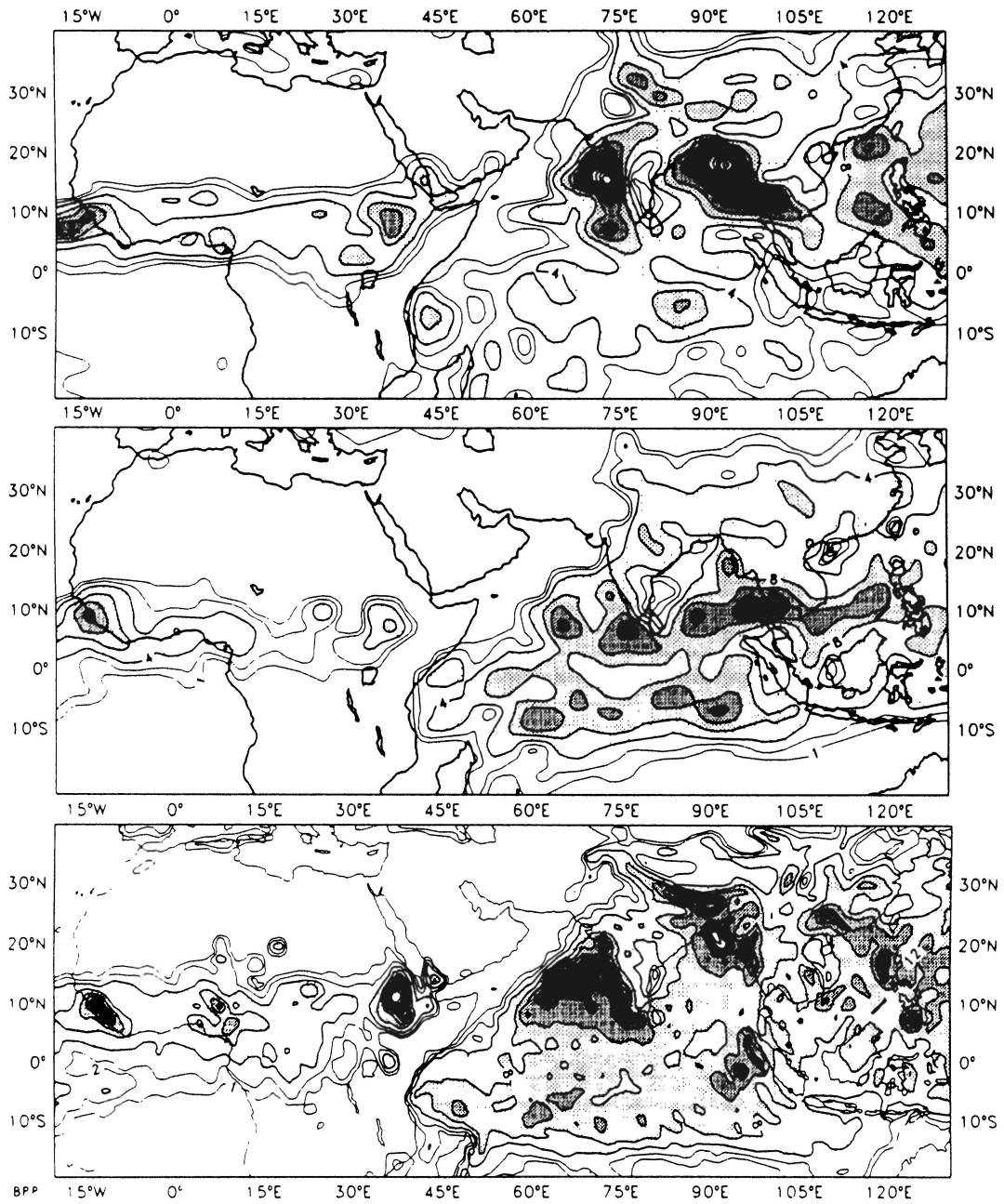

FIG. 9.13. 90-day convective precipitation for monsoon region for adjustment scheme (upper panel), operational model (center), and average of the short-range (12–36 h) forecasts (lower panel) for the same period from the operational model (T-106).

where we assume constant divergence $(\nabla \cdot \mathbf{V})_D$ of the downdraft in the BL and a constant of proportionality α. The BL time scale τ_{BL} is given by

$$\frac{1}{\tau_{BL}} = (\nabla \cdot \mathbf{V})_D = \frac{\alpha \mathrm{PR}}{\int_{p_0}^{p_{BL}} \Delta q_c \, dp/g}. \qquad (9.30)$$

This couples the BL time scale to the precipitation-driving downdraft processes. We set $\alpha = -0.25$ globally to represent a precipitation efficiency of order 0.80, consistent with tropical budget studies (Betts 1973a). The parameter could be made a function of wind shear (e.g., Fritsch and Chappell 1980). Typically τ_{BL} is longer than τ, so that the boundary-layer adjustment

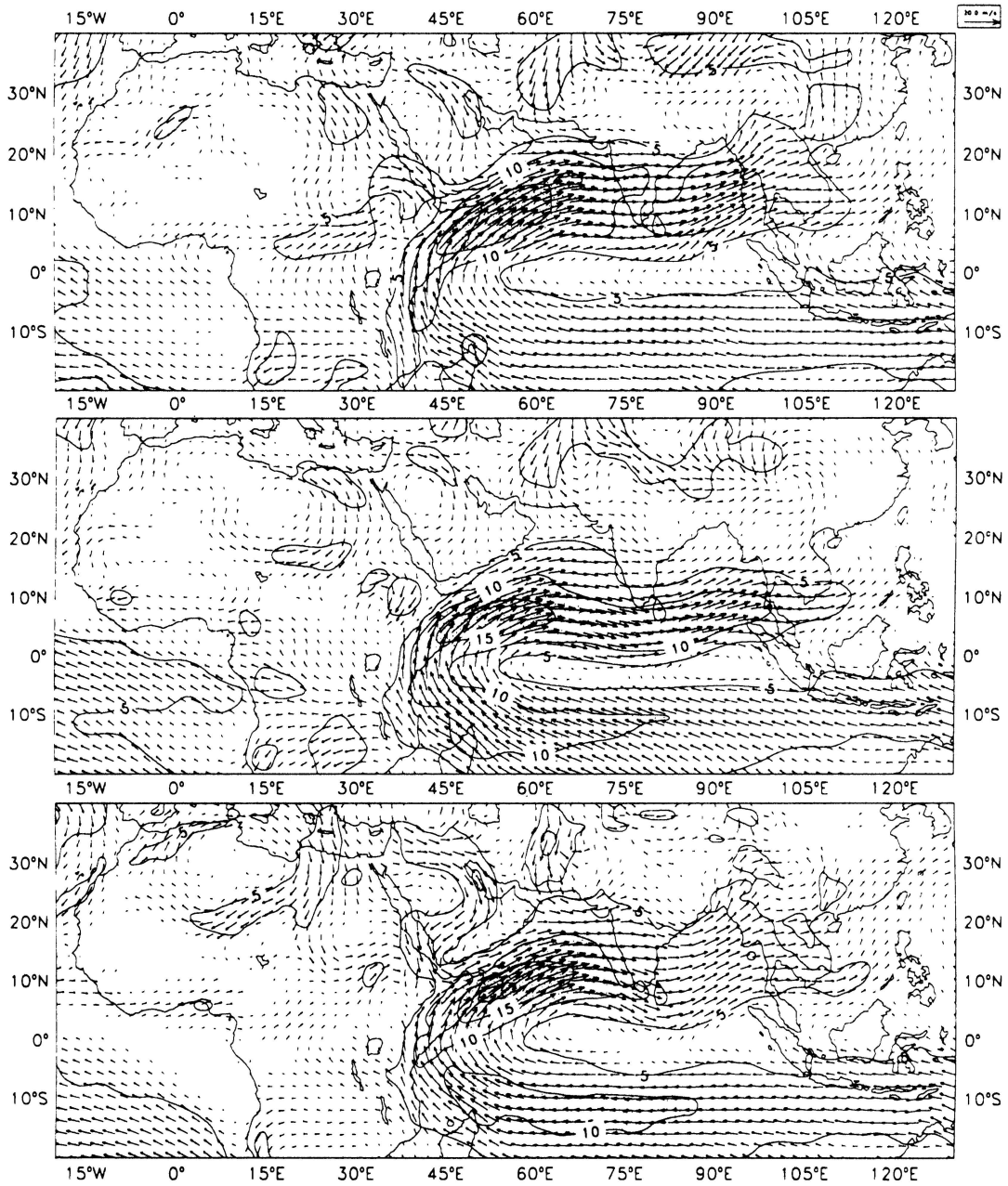

FIG. 9.14. 90-day mean flow near 850 mb for monsoon region for adjustment scheme (upper panel), operational model (center), and analysis (lower panel).

is slower and smoother than in the original version of the scheme, as well as being well defined in terms of a physical process. We have found much smoother precipitation patterns in this revised version of the scheme, presumably because the convection scheme is less apt to be shut off by rapid changes of θ_e in the BL.

c. *Modification to energy correction*

Equation (9.23) is modified to include the two adjustment time scales,

$$\Delta k = \frac{\tau}{\Delta p_c}\left[\int_{p_0}^{p_{BL}}\left(\frac{k_R - \bar{k}}{\tau_{BL}}\right)dp + \int_{p_{BL}}^{p_T}\left(\frac{k_R - \bar{k}}{\tau}\right)dp\right], \tag{9.31}$$

where p_{BL} separates the model BL from the rest of the deep convective layer. In fact, since τ_{BL} depends on the precipitation rate PR in (9.28), it is possible to formally eliminate τ_{BL} from (9.31) using (9.30) and find Δk from the reference profiles *above* the BL, as follows. The downdraft reference profiles are left un-

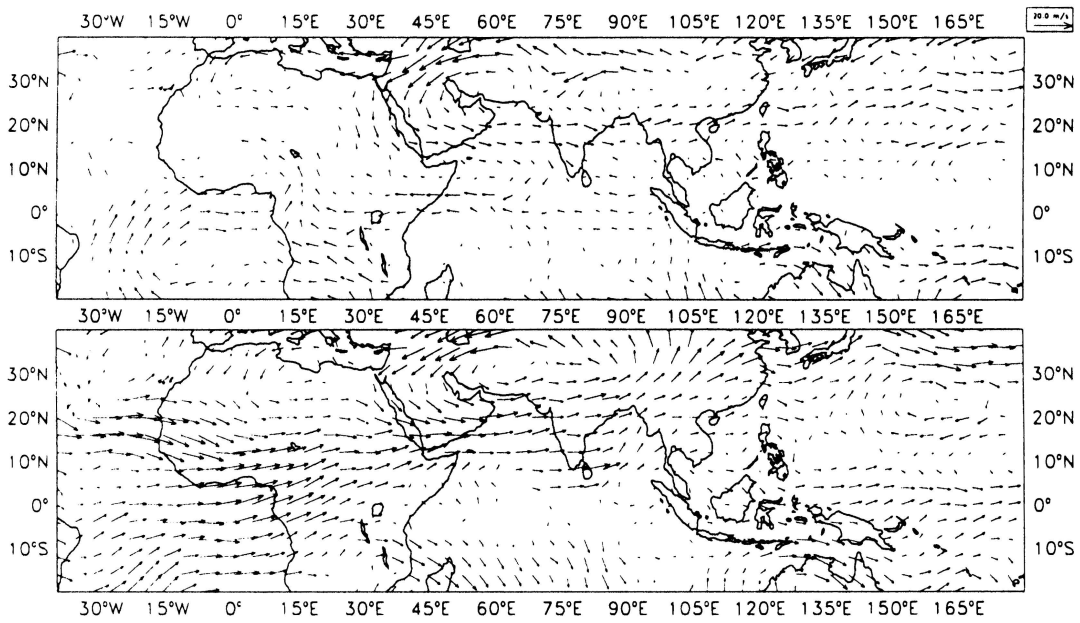

FIG. 9.15. Difference from analysis for the 200-mb flow for the adjustment scheme (upper panel) and the operational model (lower panel).

changed. Expanding (9.31) and substituting from (9.30) and (9.33) gives, after rearrangement,

$$\Delta k = \frac{1}{\Delta p_c}\left[\int_{p_{BL}}^{p_T} C_p(T_R - \bar{T})dp + \frac{1+e}{1-f}\int_{p_{BL}}^{p_T} L(q_R - \bar{q})dp\right], \quad (9.32)$$

where

$$e = \alpha C_p \int_{p_0}^{p_{BL}} \frac{(T_R - \bar{T})dp}{LE}$$

$$f = \alpha \int_{p_0}^{p_{BL}} \frac{(q_R - \bar{q})dp}{E}$$

and $E = \int_{p_0}^{p_{BL}} \Delta q_c dp$ is part of (9.29). Note that the terms f and e (which are both defined positive) can be zero if either $\alpha = 0$ (the prescribed ratio of evaporation to precipitation) or if (9.28) are satisfied in some integral sense (an internal adjustment).

Once the energy correction is made, the precipitation can be calculated:

$$\mathrm{PR} = \int_{p_0}^{p_{BL}} \frac{(q_R - \bar{q})}{\tau_{BL}} \frac{dp}{g} + \int_{p_{BL}}^{p_T} \frac{(q_R - \bar{q})}{\tau} \frac{dp}{g} = \left(\int_{p_{BL}}^{p_T} \frac{q_R - \bar{q}}{\tau} \frac{dp}{g}\right) \frac{1}{1-f}. \quad (9.33)$$

Typically, for $\alpha = -0.25$, f and e are small with $f \leq 0.2$ and $e < 0.1$.

9.5. Impact of scheme on the tropical summer climate in the ECMWF model

We shall illustrate the impact of the scheme using a 90-day summer run made at T-42 triangular truncation with cycle 38 of the ECMWF model. We show comparisons between the operational model, which uses Tiedtke's (1989) mass flux scheme with a boundary-layer moisture convergence closure, and a parallel run with the current version of the Betts–Miller scheme discussed in sections 9.3 and 9.4. This comparison will illustrate both the impact of a different convection scheme on the tropical climate of a model and the complexity of understanding the interactions between convection and the large-scale fields in a global model.

This 90-day T-42 forecast was initialized with atmospheric data from 1 June 1988 and with observed sea surface temperatures updated every five days. We will present averages from days 1 to 90 for selected fields and compare them with a parallel run from the same initial conditions using the operational model (cycle 38). Figure 9.12 shows the global pattern of convective precipitation from the two simulations: for the adjustment scheme (upper panel) and for the operational scheme (lower panel). We see significant differences in several areas of the globe. In the northeastern Pacific the maximum in the precipitation in the tropical convergence zone is shifted off the coast with the Betts–Miller scheme. Over the tropical continents, the precipitation is somewhat enhanced. The biggest difference, however, is in the Indian monsoon circulation, where the climate with the adjustment scheme has a strong monsoon flow giving the typical

monsoon precipitation on the northwest coast of India (e.g., Grossman and Durran 1984; Grossman and Garcia 1990). Figure 9.13 shows the Indian monsoon region on a larger scale with three panels. The lower panel is an average of 90 short-range precipitation forecasts (12–36 h) from the operational forecast model at T-106 for the relevant period. The upper panel is from the 90-day T-42 forecast with the adjustment scheme. The agreement with the average of the short-range forecasts for the same period is striking. The middle panel is the 90-day T-42 forecast with the operational model: we see that it clearly drifts to a tropical climate that has a weak monsoon. Figure 9.14 compares the flow near 850 mb for the 90-day average of the analysis (lower panel) with the two 90-day forecasts. The adjustment scheme 90-day climate (upper panel) has a much stronger southwesterly monsoon, somewhat stronger than the analysis, which impinges on the Western Ghat Mountains, producing the precipitation pattern shown in Fig. 9.13. In contrast the 850-mb flow in the Indian Ocean for the climate of the operational model (middle panel) has appreciable differences from the analysis, with the main branch of the southwesterly monsoon flow passing to the south of India and an increase in the flow across 20°S. This change in the low-level monsoon circulation has a big impact on the upper-level flow. Figure 9.15 shows the difference from the analysis for these 90-day averages for the 200-mb flow for this region and farther east. The operational model, which has too weak a monsoon circulation (in the 90-day climate), has large wind errors at 200 mb. With the adjustment scheme the upper-level wind errors are greatly reduced because the monsoon circulation and precipitation are improved. From a climate modeling viewpoint these changes are significant, but what features of the different convection schemes are responsible for the differences in climate? This is a difficult question to answer. The interaction between the climatic scale, the synoptic-scale disturbances, and the convection scheme occurs within a few days in the tropics, and the model circulation shifts to a different state.

Despite almost two decades since the planning of the GATE experiment (Betts 1974a), more research is still needed to understand the interaction between convection and the larger scales in the tropics.

Acknowledgments. This work was supported by the National Science Foundation under Grant ATM-9001960, the NASA Goddard Space Flight Center under Contracts NAS5-30524 and NAS5-31738, and by ECMWF, while the first author was a visiting scientist.